Cell-assembled nanoclusters of MSC–targeting Gd–DOTA–peptide as a T2 contrast agent for MRI cell tracking

Article *in* Journal of Peptide Science · February 2018

DOI: 10.1002/psc.3077

CITATIONS
6

READS
63

7 authors, including:

Yanhui Zhang
Institute of Nano-tech and Nano-bionics, Chinese Academy of Sciences, Suzhou ,…
10 PUBLICATIONS 65 CITATIONS

Hailu Zhang
Chinese Academy of Sciences
91 PUBLICATIONS 2,771 CITATIONS

RESEARCH ARTICLE

WILEY *Journal of* PeptideScience

Cell-assembled nanoclusters of MSC-targeting Gd-DOTA-peptide as a T_2 contrast agent for MRI cell tracking

Pengli Zhang[1,2] | Yanhui Zhang[2] | Binbin Li[2] | Hailu Zhang[2] | Haixia Lin[1] | Zongwu Deng[2] | Bo Tan[2] [iD]

[1] College of Sciences, Shanghai University, Shanghai 200444, China

[2] CAS Key Laboratory of Nano-Bio Interface and Division of Nanobionics Research, Suzhou Institute of Nano-Tech and Nano-Bionics, Chinese Academy of Sciences, Suzhou 215123, China

Correspondence
Bo Tan, CAS Key Laboratory of Nano-Bio Interface and Division of Nanobionics Research, Suzhou Institute of Nano-Tech and Nano-Bionics, Chinese Academy of Sciences, Suzhou 215123, China.
Email: btan2012@sinano.ac.cn

A cyclic peptide CC9 that targets cell membrane of mesenchymal stem cells (MSCs) is coupled with Gd-DOTA to yield a Gd-DOTA-CC9 complex as MRI contrast agent. It is used to label human MSCs (hMSCs) via electroporation. Electroporation-labeling of hMSCs with Gd-DOTA-CC9 induces cell-assembly of Gd-DOTA-CC9 nanoclusters in the cytoplasm, significantly promotes cell-labeling efficacy and intracellular retention time of the agent. In vitro MRI of labeled hMSCs exhibits significant signal reduction under T_2-weighted MRI, which can allow long-term tracking of labeled cell transplants in in vivo migration. The labeling strategy is safe in cytotoxicity and differentiation potential.

KEYWORDS
cell tracking, MRI, MSC targeting peptide, nanocluster, self-assembly

1 | INTRODUCTION

Magnetic resonance imaging (MRI) has been subjected to intensive investigation as a noninvasive visualizing tool for tracking of stem cells in survival, migration and homing, differentiation, and other physiological activities.[1-3] The transplanted cells are usually labeled with MRI contrast agents (CAs), which, combined with an appropriate imaging mode, distinguishes the labeled cells from their surrounding tissue in vivo.[4,5] Superparamagnetic iron oxide nanoparticles have been extensively studied for stem cell labeling and tracking under T_2-weighted MRI over the past 2 decades.[5,6] However, several inherent limitations have been recognized for this labeling strategy. For example, superparamagnetic iron oxide nanoparticles released from dead cells are cleared slowly in vivo, and its uptake by other cells such as macrophages may lead to image misinterpretation. T_2-weighted images are also subjected to "artifact" interference in vivo.[7,8] On the other hand, cell labeling with Gd-based CAs that is in favor of T_1-weighted MRI and can avoid "artifact" interference has also received broad research interest for stem cell tracking.[8,9] However, it also faces several limitations, including limited signal enhancement effect of various Gd agents and short intracellular retention time (ICRT) of small molecule Gd agents.[10]

Recently, we reported that cell labeling with a mitochondria-targeting Gd-based CA (Gd-DOTA)$_i$-TPP via electroporation (EP) induces self-assembly of intracellular (Gd-DOTA)$_i$-TPP nanoclusters.[11] The labeling strategy significantly promotes ICRT of the CA and allows long-term tracking of the labeled cells with T_2-weighted MRI. Abundant information on in vivo fates of cell transplants can be revealed.[11,12] In this respect, Gd-DOTA was coupled with a mitochondria-targeting moiety in attempt to promoting its ICRT. However, it turns out that its ICRT is significantly promoted by the formation of intracellular nanoclusters induced by EP-labeling instead of binding to mitochondria. Transmission electron microscopy (TEM) observation further revealed a possible formation process: The (Gd-DOTA)$_i$-TPP probes first bound ubiquitously on the cell membrane, then EP induced clustering of the probes on the cell membrane, which further proceeded with the formation of intracellular nanoclusters.[11]

A question is immediately raised as whether ICRT can also be promoted by EP-labeling when Gd-DOTA is coupled with a cell membrane-targeting moiety. Many peptides have been used as cell-targeting moiety of MRI CAs.[13-17] Recently, several peptide sequences have been reported to bind specifically with mesenchymal stem cells (MSCs).[18,19] In a previous work,[20] we have coupled Gd-DOTA with a peptide CC9 that targets cell membrane of MSCs as well as a cell-penetrating peptide (TAT) as MRI CAs. We have reported their T_1-weighted MRI signal enhancement effect resulting from cell labeling via cell culture in the presence of the CAs. However, the signal

enhancement effect cannot persist long enough for in vivo cell tracking. Prompted by our latest findings,[11,12] we set out to investigate whether EP-labeling of cells with Gd-DOTA-CC9 can also induce cell-assembly of intracellular nanoclusters and promote its ICRT. CC9 is a cyclic peptide with a sequence of Cys(disulfide bridge)-Ser-Thr-Asn-Pro-Lys-Val-Leu-Cys(disulfide bridge) that targets cell membrane of MSCs.[19] We report both the cytotoxicity of the labeling strategy and the potential of using this strategy for long-term tracking of stem cell transplants.

2 | MATERIALS AND METHODS

2.1 | Materials

1,4,7,10-Tetraazacyclododecane hydrochloride was purchased from Shanghai Titan Scientific Co. Ltd. (China). Other chemicals were purchased from Sinopharm Chemical Reagent Company (China). All chemicals are of analytical grade. Annexin V-FITC Apoptosis Detection Kit was purchased from Becton, Dickinson and Company (BD, USA). Cell Viability Assay Kit (MTT), lactate dehydrogenase (LDH) Cytotoxicity Assay Kit, and Reactive Oxygen Species Assay Kit (ROS) were purchased from Beyotime (China). Fetal bovine serum, DMEM-F12 medium, penicillin-streptomycin, pancreatin, and all cell culture related reagents were purchased from Gibco (USA). Milli-Q water (18.2 M Ω cm^{-1}) was used throughout the experiments.

2.2 | Synthesis and characterization of Gd-DOTA-CC9

Chemical structure of Gd-DOTA-CC9 is illustrated in Figure 1. 1-(Acetic acid)-4,7,10-tris (tert-butoxycarbonyl methyl)-1,4,7,10-tetraazacyclo-dodecane (DOTA(O^{t}Bu)$_3$) was synthesized by a multistep procedure from cyclen hydrochloric salt according to literature[21] and was used for solid phase synthesis of DOTA-CC9. Details on synthesis and characterization of DOTA-CC9 and Gd-DOTA-CC9 can be found elsewhere.[11,20] Their molecular weights were determined by electron-stimulated ionization mass spectrometry (Agilent 1200/6220).

2.3 | Cell culture and labeling

2.3.1 | Culture of human MSCs

Human MSCs (hMSCs) were obtained as a generous gift from Dr Jianwu Dai at Institute of Genetics and Developmental Biology, Chinese Academy of Sciences. hMSCs were cultured at 37°C in a 5% CO_2 incubator (Thermo 3111, MA, USA) in DMEM-F12 medium with 10% fetal bovine serum and 1% penicillin-streptomycin. hMSCs were seeded into 100 × 20-mm style cell culture dishes at a density of about 1 × 10^6 cells per dish and maintained for 24 hours.

2.3.2 | EP-labeling of hMSCs with Gd-DOTA-CC9

hMSCs were trypsinized and centrifuged at 1000 rpm for 5 minutes. The precipitated cells were resuspended in 200-µL EP-buffer in the presence of Gd-DOTA-CC9 at concentrations of 0.0, 0.5, 1.0, 2.0, and 4.0 mM, respectively, and were then transferred into 96-well plates. Six electrical pulses of 100 µs at ~120 V and an interval of 1 second were then applied to the cells by using X-Porator® EBXP-H1 (Etta Biotech, China). After EP-labeling, cells were rinsed twice with 4 to 6-mL phosphate-buffered saline (PBS) to remove the residual materials and were then transferred into 100 × 20 mm dishes for incubation and proliferation.

2.3.3 | Gd quantification in hMSCs

Cellular Gd content was determined by inductively coupled plasma mass spectrometry (ICP-MS, Thermo X Series2, USA). After counted by a hemocytometer, hMSCs labeled with Gd-DOTA-CC9 were digested overnight by using 0.5 mL of concentrated nitric acid and 0.5 mL of 30% hydrogen peroxide. Samples were then diluted to a total volume of 5 mL with deionized water and analyzed by ICP-MS, from which total Gd content was derived. Cellular Gd content was determined by dividing total Gd content by using the counted cell number. The measurements were repeated 3 times, and the mean value was reported.

2.4 | Cytotoxicity assessment of EP-labeled hMSCs

2.4.1 | Apoptosis and necrosis assay

Apoptosis and necrosis of hMSCs induced by Gd-DOTA-CC9 were assessed immediately after EP-labeling by using an apoptosis and necrosis assay kit. hMSCs EP-labeled with Gd-DOTA-CC9 at concentrations of 0.0, 0.5, 1.0, 2.0, and 4.0 mM, respectively, were seeded in 6-well plates (2 × 10^5 cells per well). hMSCs without EP-labeling were used as a control. Cells were harvested when their density grew to 80%, resuspended in V-FITC binding buffer, and incubated with Annexin V-FITC and PI in the dark for 20 minutes. Cell suspensions were analyzed by FACS immediately. Single-cell suspensions were analyzed by FACS (Aria II, BD, USA) within 1 hour.

2.4.2 | MTT assay

Cell viability of hMSCs after EP-labeling with Gd-DOTA-CC9 was assessed by MTT assay. Human MSCs were suspended in 200-µL EP-buffer containing 0.0, 0.5, 1.0, 2.0, and 4.0 mM of Gd-DOTA-CC9, respectively. Defined electrical pulses were applied to the cells. After EP-labeling, the cells were collected and suspended in 4-mL DMEM-F12, rinsed twice with 4 to 6-mL PBS, and transferred into a 96-well plate (8 × 10^3 cells per well). In vitro cell viability of Gd-DOTA-CC9 labeled hMSCs was assessed by using a standard MTT cytotoxicity assay.
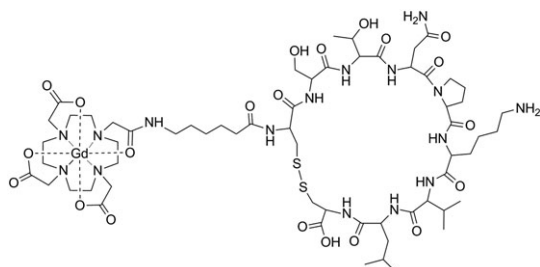
FIGURE 1 Schematic structure of Gd-DOTA-CC9

2.4.3 | LDH assay

Potential damage to the plasma membrane induced by EP-labeling with Gd-DOTA-CC9 was assessed with LDH leakage assay. hMSCs EP-labeled with Gd-DOTA-CC9 at concentrations of 0.0, 0.5, 1.0, 2.0, and 4.0 mM, respectively, were cultured overnight in 96-well plates (8×10^3 cells per well). After the cells were attached to the well, the media were collected and measured by using an LDH leakage detection kit Beyotime (China). hMSCs without EP-labeling were used as the negative control, and those treated with 1% Triton-X-100 were used as the positive control. Lactate dehydrogenase leakage of hMSCs was measured at 490 nm by using a microplate reader (Perkin Elmer Victor X, Singapore).

2.4.4 | ROS assay

hMSCs EP-labeled with Gd-DOTA-CC9 at concentrations of 0.0, 0.5, 1.0, 2.0, and 4.0 mM, respectively, were cultured in 6-well plates (2×10^5 cells per well) for cell attachment. hMSCs without EP-labeling were used for both positive and negative controls. As a positive control, hMSCs were treated with 50-mg/mL Rosup for 30 minutes at 37°C and then incubated with DCFH-DA (diluted with serum-free medium at 1:1000). Other groups were incubated only with DCFH-DA. After incubation at 37°C for 30 minutes, hMSCs were washed twice with PBS and the fluorescence of oxidized DCF was measured immediately by a microplate reader (Perkin Elmer Victor X, Singapore).

2.5 | Assessment of differentiation potent of EP-labeled hMSCs

2.5.1 | Adipogenic differentiation

For adipogenic differentiation, hMSC EP-labeled with 0, 4.0 mM Gd-DOTA-CC9 and unlabeled hMSCs were seeded in 24-well plates (1×10^5 cells per well). Upon 70% confluence, hMSCs were incubated with 1 mL adipogenic supplements consisting of 5 mg/mL insulin, 1-mM dexamethasone, 0.5 mM isobutyl methylxanthine (IBMX), and 60 mM indometacin in DMEM-F12 medium for up to 14 days with medium change every 3 days. The lipid vacuole formation in hMSCs was stained by 0.36% Oil-Red O and imaged with Nikon Ti-E microscopy (Japan). The absorbance of Oil-Red O was measured at 490 nm by using a microplate reader (Victor X, Perkin Elmer, Singapore).

2.5.2 | Osteogenic differentiation experiment

For osteogenic differentiation, EP-labeled and unlabeled hMSCs were incubated with 1-mL osteogenic supplements consisting of 0.05 mg/mL ascorbic acid, 100 nM dexamethasone, and 0.01 M bglycerophosphate in DMEM-F12 medium for up to 21 days with medium change every 3 to 4 days. Differentiation of hMSCs into osteogenic cells was determined by 0.2% alizarin red staining. Osteogenic differentiation of hMSCs was quantified by measuring the absorbance of alizarin red extracted from cell lysates at 490 nm (Victor X, Perkin Elmer, Singapore).

2.6 | TEM of EP-labeled hMSCs

Transmission electron microscopy was performed to disclose cellular distribution of Gd-DOTA-CC9. EP-labeled hMSCs were directly fixed in dish with 2.5% glutaraldehyde for 6 hours at 4°C, washed twice with PBS, scraped gently with a cell scraper and transferred to a 15 mL centrifuge tube, rinsed twice in PBS, and centrifuged at 1000 rpm for 5 minutes; the supernatant was removed. Afterward, the cell mass was embedded in 5% agar gel and fixed in 2.5% glutaraldehyde buffered with PBS at 4°C for at least 6 hours followed by washing with PBS twice. The cells were then fixed in 1% osmium tetraoxide buffered with PBS for 1 hour and washed 3 times with PBS. The samples were dehydrated by using a series of acetone treatment (30%, 50%, 70%, 80%, 90%, and 3 × 100%) of 15 minutes each, followed by embedded in 1:1 epoxy resin/acetone solution for 1 hour. The samples were then transferred into capsules containing fresh 100% epoxy resin for at least 2 hours. The capsules were left in a furnace at a temperature of 70°C for 2 days to polymerize the epoxy resin. After quickly cooling down, the hardened samples were cut into sections 70 to 90 nm thick with ultramicrotome (Leica UC6, Austria) and applied on a copper grid for TEM observation (HT7700, Hitachi High-Technologies Corporation, Japan).

2.7 | In vitro MR imaging of EP-labeled hMSCs

hMSCs EP-labeled with Gd-DOTA-CC9 at concentrations of 0, 0.5, 1.0, 2.0, and 4.0 mM were seeded in 100 × 20 mm dish (~1×10^6 cells/dish). When cell density grew to 90%, half of labeled hMSCs were used for proliferation and the other half were treated for in vitro MRI. For MRI, hMSCs were trypsinized, centrifuged, and washed twice with PBS. The harvested cells were transferred into a capillary of 0.9 to 1.1 mm inner diameter and packed into cell pellets by centrifugation at 1200 rpm for 5 minutes. T_1- and T_2-weighted images of hMSC pellets were collected on an 11.7 T NMR spectrometer (Bruker-Biospin, Gemany). T_1 and T_2 relaxation times were also measured.

T_1-weighted images were acquired by using MSME sequence with T_E = 5.2 ms, T_R = 500 ms, FOV = 12 × 12 mm^2, matrix = 96 × 96, slice thickness/gap = 0.8/0.2 mm, and number of average = 4. T_2-weighted images were acquired by using MSME sequence with T_E = 40 ms, T_R = 3000 ms, FOV = 12 × 12 mm^2, matrix = 96 × 96, slice thickness/gap = 0.8/0.2 mm, and number of average = 2.

T_1 relaxation time were acquired by using RARE sequence with T_E = 7 ms; T_R = 40, 70, 100, 180, 300, 500, 750, 1000, 1500, 3000, 5000 ms; FOV = 12 × 12 mm^2; matrix = 96 × 96; slice thickness/gap = 0.8/0.2 mm; and number of average = 2. T_2 relaxation time were acquired by using MSME sequence with T_R = 3000 ms, T_E = 8 to 480 ms, FOV = 12 × 12 mm^2, matrix = 96 × 96, slice thickness/gap = 0.8/0.2 mm, and number of average = 2.

2.8 | In vivo MR imaging examination

Animal handling was carried out at the animal laboratory of Soochow University, China. All animal experiments were conducted in accordance with the university's guidelines and were approved by the university's ethics committee.

hMSC EP-labeled with Gd-DOTA-CC9 were harvested by trypsinization and re-suspended in PBS. Male nude mice (5-6 weeks old) with body weight of 20 to 25 g were bought from Lingchang

biotechnology Co. Ltd (Shanghai, China) and were anesthetized by intraperitoneal injection of 5% chloral hydrate solution at a dose of 7.5-mL/kg body weight and then fixed onto a stereotaxic apparatus. Defined number of labeled hMSCs ($3\text{-}4 \times 10^5$ cells) in 5-μL PBS was injected into the left brain hemisphere of the nude mice (n = 3) at a rate of 0.5 μL/min by using a Hamilton microsyringe with a 27-gauge needle. The needle was left in place for an additional 5 minutes before it was withdrawn to reduce the protraction of the cells into the needle track. The burr hole was filled with bone wax, and the scalp was closed with sutures. The right brain hemisphere with no cell injection was used as a control. The nude mice were then transferred and fixed into an animal handling system coupled with a Micromouse RF probe (Bruker, Germany). They were then inserted into the 11.7 T microimaging system for in vivo MRI.

2.9 | Gadolinium concentration in organs, urine, and feces

Mice feces and urine were collected from the metabolic cages every 4 days to determine relative Gd concentration. After the last in vivo MRI on day 12, the animals were sacrificed. Lungs, livers, and kidneys were excised to determine the remaining Gd content in these organs.[8] All samples were digested overnight by using nitric acid and were then diluted to a total volume of 5 or 10 mL with deionized water and analyzed by ICP-MS.

3 | RESULTS AND DISCUSSION

3.1 | Synthesis and characterization of Gd-DOTA-CC9

Figure 1 illustrates chemical structure of Gd-DOTA-CC9. The structure was determined by controlling the sequence of adding amino acid during solid phase synthesis of DOTA-CC9 and was confirmed by their molecular weights as measured by electron-stimulated ionization mass spectrometry. Figure S1 showed mass spectrum of DOTA-CC9 ($C_{61}H_{104}N_{16}O_{21}S_2$, exact mass [100%]: 1460.70), found m/z 1461.8 for $[M + H]^+$, 731.1 for $[M + 2H]^{2+}$, 487.8 for $[M + 3H]^{3+}$; Figure S2 showed high resolution mass spectrum of Gd-DOTA-CC9 ($C_{61}H_{101}GdN_{16}O_{21}S_2$, exact mass [100%]: 1615.6010), found m/z 1616.6084 for $[M + H]^+$, 808.8095 for $[M + 2H]^{2+}$. The measured aqueous r_1 and r_2 of Gd-DOTA-CC9 are 7.75 and 11.48 $\text{mM}^{-1} \text{ s}^{-1}$ at 11.7 T as shown in Figure S3.

3.2 | EP-labeling efficacy and dilution of cellular Gd content

Figure 2 presents cellular Gd content of hMSCs EP-labeled with Gd-DOTA-CC9 at different concentrations as functions of cell proliferation time. Cellular Gd content of EP-labeled hMSCs increased from $\sim 3 \times 10^9$ Gd/cell to $\sim 5 \times 10^{10}$ Gd/cell with increase of Gd-DOTA-CC9 concentration from 0.5 to 4.0 mM. In the subsequent proliferation, cellular Gd content exhibited a gradual decrease as a result of exocytosis and cell division. After 10 days of proliferation, cellular Gd content of hMSC EP-labeled at 4.0mM Gd-DOTA-CC9 remained $\sim 4 \times 10^9$ Gd/cell.
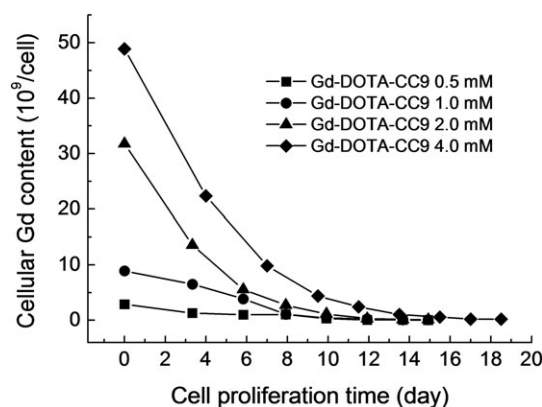
FIGURE 2 Cellular Gd content of human mesenchymal stem cell electroporation-labeled at different Gd-DOTA-CC9 concentrations as functions of cell proliferation time

3.3 | Cytotoxicity of Gd-DOTA-CC9 on EP-labeled hMSCs

The potential cytotoxicity of Gd-DOTA-CC9 was assessed by apoptosis and necrosis, MTT, LDH, and ROS assays. Apoptosis and necrosis of hMSCs were assessed immediately after EP-labeling of hMSCs. No significant apoptosis or necrosis was induced by EP-labeling of hMSCs with Gd-DOTA-CC9 at concentrations of 0.5 to 2.0 mM (Figure 3A). The normal cells represented ~95% of total cells for control hMSCs and 85 to 90% of total cells for hMSCs subjected to EP0 to EP2. hMSCs subjected to EP4 show more than 50% normal and ~38% necrosis of total cells.

MTT, LDH, and ROS of hMSCs were assessed after a 2 to 3 day recovery following EP-labeling. MTT assay (Figure 3B) shows that EP conducted on hMSCs in the absence of CA exerted minor adverse effects on the survival of hMSCs with cell viability of ~85% (EP0); no additional adverse effect was induced by the introduction of Gd-DOTA-CC9 at concentrations of 0.5 to 4.0 mM (EP0.5-EP4).

Lactate dehydrogenase assay (Figure 3C) shows that all EP-labeled hMSCs exhibited no obvious change in LDH leakage compared with control hMSCs. Lactate dehydrogenase leakage was much lower than the positive group treated with 1% Triton-X-100, indicating that EP-labeling exerted no obvious damage to cell membrane of hMSCs.

High intracellular ROS value would lead to cellular oxidative stress and causes damage to DNA, protein, and other biological macromolecules of cells. Cellular ROS could be determined by measuring intracellular DCF content because nonfluorescent DCFH could be oxidized to fluorescent DCF by ROS. DCF content (Figure 3D) of hMSCs subjected to EP0 to EP4 was at a similar level to that of control hMSCs and was much lower than that of the positive control treated with Rosup. The results suggest that both the EP-labeling and cellular uptake of Gd-DOTA-CC9 at 0.5 to 4.0 mM are tolerable by hMSCs. An increase in necrosis occurred to EP-labeling at 4.0 mM, but the viable cells remained normal in MTT, LDH, and ROS assays.

3.4 | Differentiation potential of EP-labeled hMSCs

The effect of EP-labeling and cellular uptake of Gd-DOTA-CC9 on adipogenic and osteogenic differentiation of hMSCs is shown in Figure 4. hMSCs EP-labeled with Gd-DOTA-CC9 at 4.0 mM were
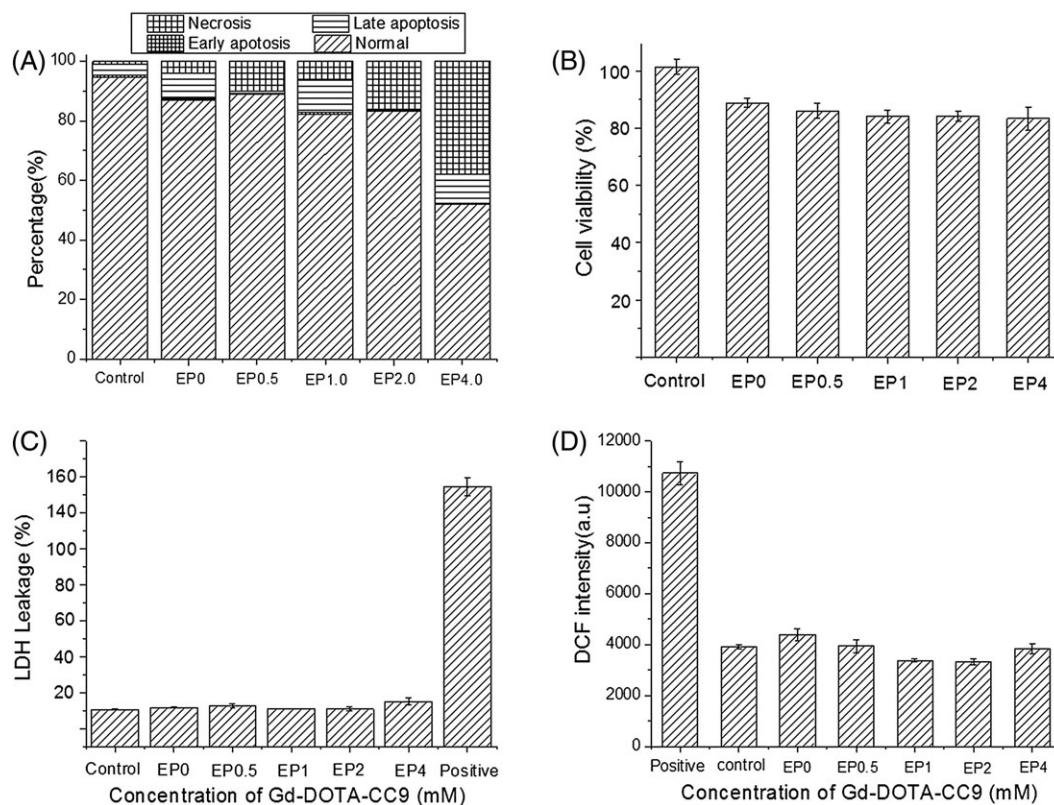
FIGURE 3 Apoptosis and necrosis (A), MTT (B), LDH (C), and ROS (D) assays of human mesenchymal stem cell electroporation-labeled with Gd-DOTA-CC9

cultured in the presence of adipogenic supplements for 14 days, then stained with 0.36% oil red O. Red lipid vacuole was clearly observed for both differentiated control hMSCs (Figure 4A/a2) and hMSCs subjected to EP in the absence (Figure 4A/a3) and presence of Gd-DOTA-CC9 (Figure 4A/a4) with respect to the undifferentiated control hMSCs (Figure 4A/a1). Quantitative analysis of the oil red O extracted from adipogenic cells revealed significantly higher level of absorbance at 490 nm for hMSCs subjected to EP than for the undifferentiated control (Figure 4C).

For osteogenic differentiation, hMSCs were treated with osteogenic supplements for 21 days, followed by 0.2% alizarin red staining. Red calcium mineral nodules were clearly observed for both differentiated control hMSCs (Figure 4B/b2) and hMSCs subjected to EP in the absence (Figure 4B/b3) and presence of Gd-DOTA-CC9 (Figure 4B/b4) with respect to the undifferentiated control hMSCs (Figure 4B/b1). Quantitative analysis of oil alizarin red extracted from osteogenic cells revealed significantly higher level of absorbance at 490 nm for hMSCs subjected to EP than for the undifferentiated control (Figure 4D). The results suggest that neither EP nor cellular uptake of Gd-DOTA-CC9 exerted adverse effect on differentiation of hMSCs into adipocytes or osteocytes.

3.5 | Cellular distribution of Gd-DOTA-CC9 in EP-labeled hMSCs

Transmission electron microscopy discloses intracellular distribution and aggregation of Gd-DOTA-CC9 in the cytoplasm of hMSCs (Figure 5). Formation of Gd-DOTA-CC9 nanoclusters in the cytoplasm was clearly

observed. The nanoclusters had a size from hundreds of nanometers to several micrometers and consisted of many nanoneedles with a length of 20 to 50 nm and diameter ~5 nm. Formation of the intracellular nanoclusters likely proceeded with a similar process as already described elsewhere.[11] It started with a ubiquitous binding of Gd-DOTA-CC9 to the cell membrane associated with its binding affinity to MSCs.[19] The backbone cyclic structure of CC9 that formed through disulfide bridge exhibited a high binding efficacy to cell membrane.[22] Electroporation induced its clustering on the cell membrane, which further proceeded with the formation of intracellular nanoclusters. We note that certain amount of free Gd-DOTA-CC9 was also introduced into the cytoplasm during EP-labeling as well described in literature.[23] As a result, EP introduced 2 different forms of Gd-DOTA-CC9 into hMSCs which contributed to MRI signals in different ways as discussed below. The free Gd-DOTA-CC9 agents were quickly released via an exocytosis process in subsequent cell proliferation, whereas the intracellular nanoclusters had longer ICRT which render long-term tracking of stem cell transplants, as confirmed by in vitro MRI experiments.

3.6 | In vitro MRI of EP-labeled hMSCs

Figure 6 shows T_1- and T_2-weighted MR images of hMSC EP-labeled with Gd-DOTA-CC9 at concentrations of 0.5, 1.0, 2.0, and 4.0 mM collected immediately after cell labeling as well as subsequently after cell proliferation of defined times. The T_1-weighted images (Figure 6A) exhibited obvious bright signals only for the hMSCs collected immediately after cell labeling at 0.5 and 1.0 mM Gd-DOTA-CC9. No T_1-weighted signal enhancement was observed for hMSCs EP-labeled
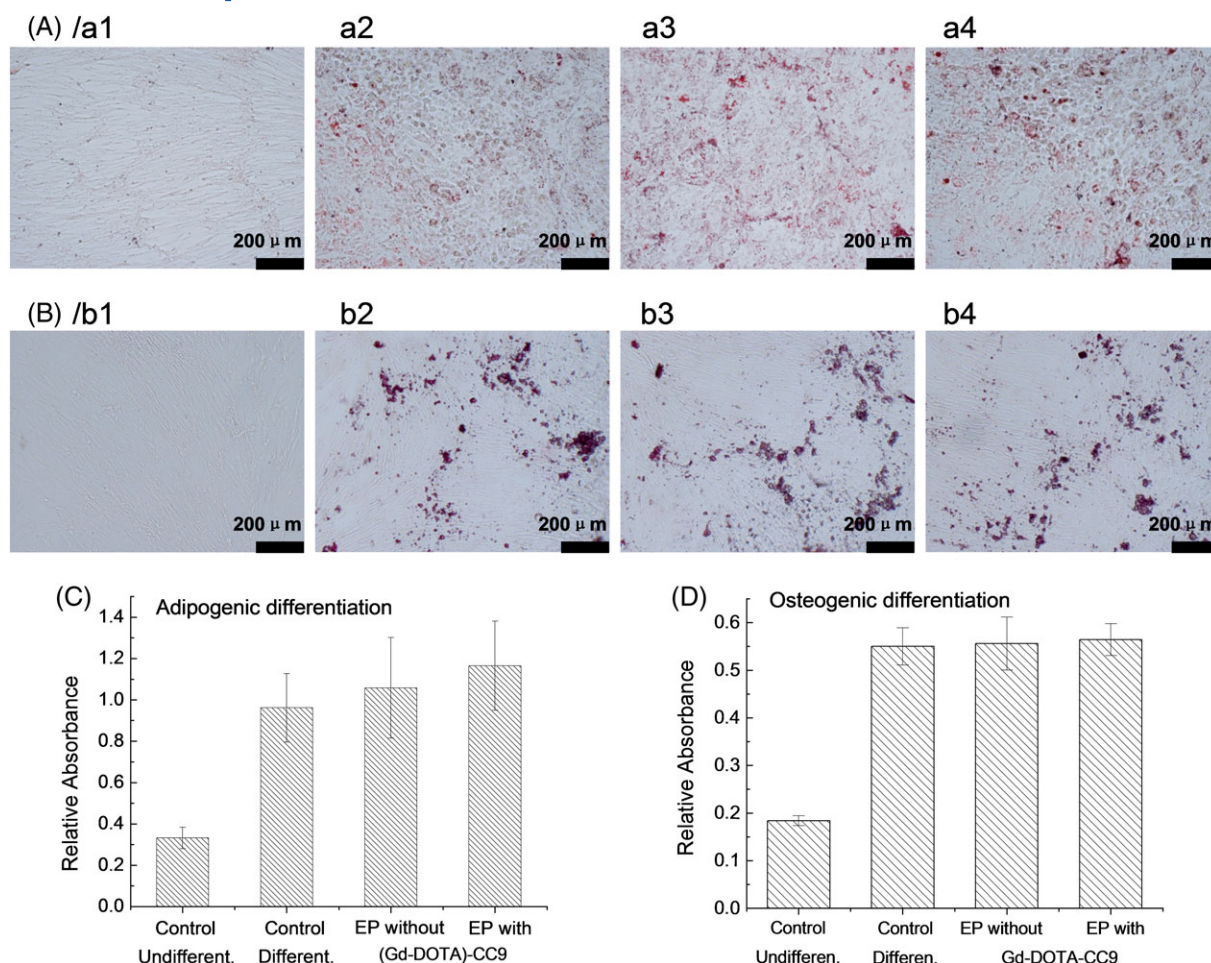
FIGURE 4 Effects of (electroporation) EP-labeling and cellular uptake of Gd-DOTA-CC9 on adipogenic (A) and osteogenic (B) differentiation of human mesenchymal stem cells (hMSCs). Nondifferentiated control hMSCs (a1/b1), differentiated control hMSCs (a2/b2), and differentiated hMSCs subjected to EP in the absence (a3/b3) and presence (a4/b4) of 4.0 mM Gd-DOTA-CC9. Quantification of adipogenic (C) and osteogenic (D) differentiation was conducted by measuring the absorbance of oil-red O and alizarin red extracted from cell lysates at 490 nm, respectively
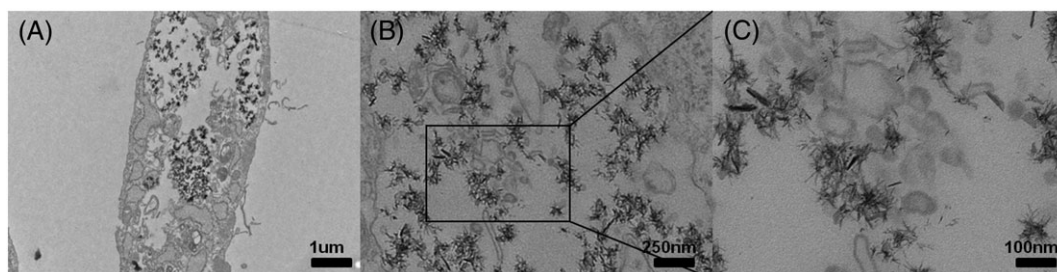

FIGURE 5 Transmission electron microscopy images of human mesenchymal stem cell electroporation-labeled with Gd-DOTA-CC9 at 4.0 mM: several nanoclusters in cytoplasm (A) and magnified structure of the nanoclusters (B and C)

at other concentrations or in subsequent cell proliferations. T_2-weighted images (Figure 6B) of hMSC EP-labeled with Gd-DOTA-CC9 at 1.0 to 4.0 mM all show significant signal reduction effect, which can persist over a long time.

The T_1- and T_2-weighted signal changes were quantified and are plotted as functions of cell proliferation time in Figure 7. hMSCs collected immediately after EP-labeling with Gd-DOTA-CC9 at 0.5 and 1.0 mM concentrations exhibited obvious T_1-weighted signal enhancement (Figure 7A), which was quickly recovered to the level of unlabeled hMSCs in subsequent cell proliferation. T_1-weighted

signals of hMSC EP-labeled in other concentrations exhibited a similar level to that of unlabeled cells. T_2-weighted signal (Figure 7B) of all labeled hMSCs exhibited signal reduction effect, some of which reached the noise level. T_2-weighted signal exhibited a much slower recovery to the level of unlabeled cells, depending on the concentration of Gd-DOTA-CC9 during EP-labeling. We note particularly that the T_2-weighted signal reduction of hMSC EP-labeled with Gd-DOTA-CC9 at 4.0 mM persisted over 2 weeks.

Figure 7C and D presents T_1- and T_2-relaxation rates of hMSCs measured after MR image collection as a function of cell proliferation
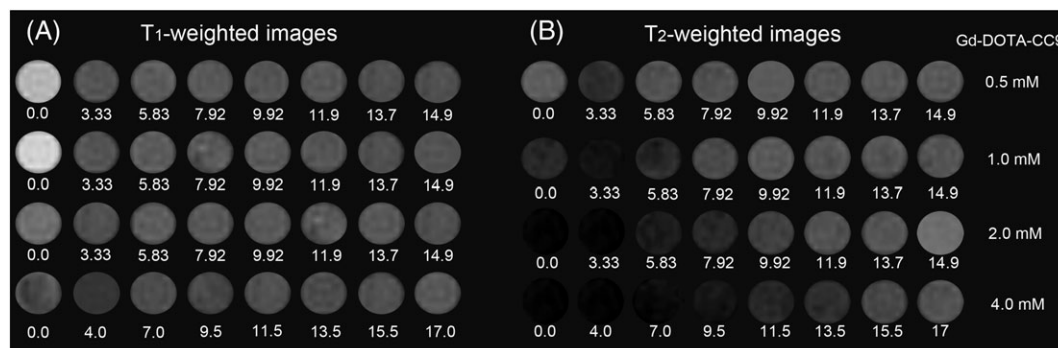
FIGURE 6 In vitro T_1-weighted (A) and T_2-weighted (B) MR images of human mesenchymal stem cell pellet electroporation-labeled with Gd-DOTA-CC9 as functions of cell proliferation time at 11.7 T. The number below each image indicates cell proliferation time in day
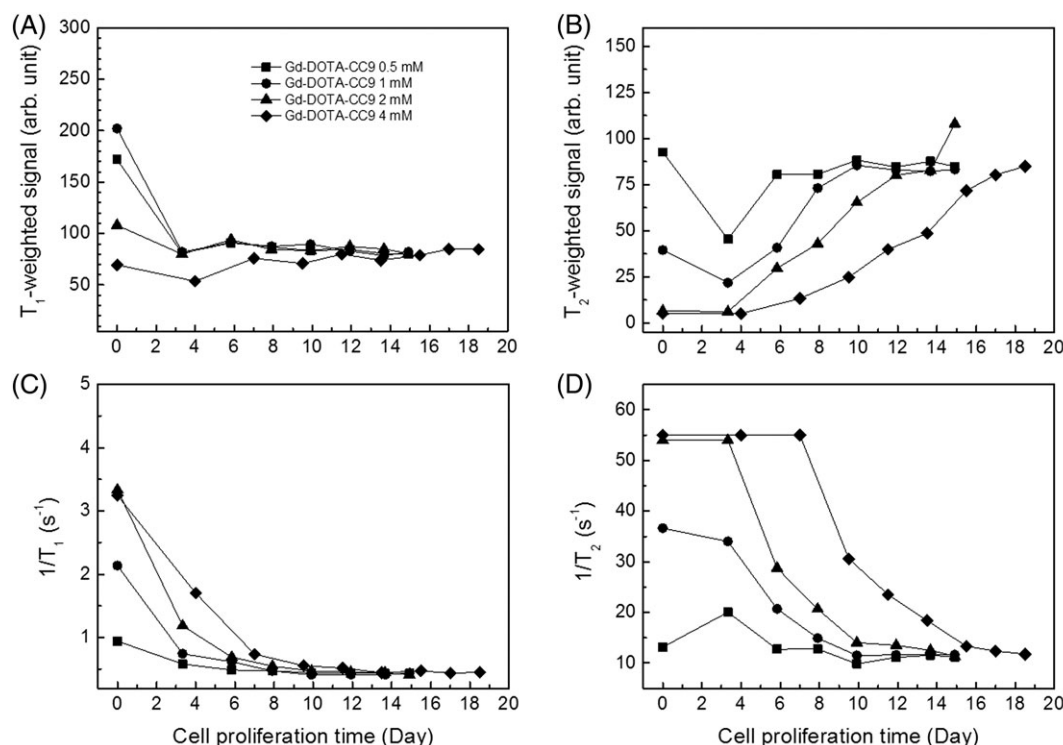
FIGURE 7 T_1-weighted (A) and T_2-weighted (B) MRI signal, T_1-relaxation (C) and T_2-relaxation (D) rates of human mesenchymal stem cell electroporation-labeled with Gd-DOTA-CC9 at different concentrations as functions of cell proliferation time. MR signal intensity of dark image is tentatively given a value of 5 or below for ease of following its change profile (B). Discussion on T_2 relaxation rate has to be restricted to below 50 because the accuracy of measurement of T_2 relaxation rate deteriorates at above 50 (equivalent to T_2 relaxation time of below 20 ms)

time. T_1- and T_2-relaxation rates are defined as the inverse of T_1- and T_2-relaxation times. The measured changes in T_1- and T_2-weighted signal intensity (Figure 7A and B) can be quantitatively explained by the measured T_1- and T_2-relaxation rates (Figure 7C and D) according to Equation 1[11,24]:

$$F_{se} \propto \left(1 - e^{-T_R/T_1}\right) e^{-T_E/T_2} \qquad (1)$$

where F_{se} is the spin echo signal intensity, T_1 and T_2 are the longitudinal and transverse relaxation times, respectively, and T_R and T_E are the experimental repetition time and echo time, respectively.

Table 1 has listed selective calculations according to Equation 1 showing the relationship between MR signal intensity (only the term

of relaxation-relevance) and the relaxation rates (times) as well as the relative weight of contribution to T_1- and T_2-weighted MR signal intensities from T_1- and T_2-relaxation times. The calculations are based on the data of Figure 7 for 4.0 mM Gd-DOTA-CC9 between day 9 to 19 where T_1/T_2-weighted MR signal intensities and T_1/T_2-relaxation times are all measurable. The results demonstrate a decreasing effect (with fluctuation) from T_1-relaxation and a monotonous increasing effect from T_2-relaxtion to both T_1- and T_2-weighted MR signal intensities. Under the specific experimental conditions (T_R and T_E), the interplay of T_1- and T_2-relaxations results in a fluctuation effect on T_1-weighted signal and a monotonous recovery of T_2-weighted signal from day 9 to 19, in consistence with the measured T_1- and T_2-weighted MR signal intensities (Figure 7A and B).

TABLE 1 Selective calculations according to Equation 1 showing the relationship between MR signal intensity (only the term of relaxation relevance) and the relaxation rates (times) as well as the relative weights of contribution to T_1- and T_2-weighted MR signal intensities from T_1- and T_2-relaxation times

Relaxation Times (ms)		$(1-e^{-T_R/T_1}) \times e^{-T_E/T_2}$	
T_1	T_2	T_1-weighted (T_R = 500 ms, T_E = 5.2 ms)	T_2-weighted (T_R = 3 s, T_E = 40 ms)
1794	32.7	0.243 × 0.853 = 0.207[a]	0.812 × 0.294 = 0.239
1937	42.5	0.228 × 0.885 = 0.202	0.788 × 0.390 = 0.307
2251	54.3	0.199 × 0.909 = 0.181	0.736 × 0.479 = 0.353
2114	75.1	0.211 × 0.933 = 0.197	0.758 × 0.587 = 0.445
2269	80.8	0.198 × 0.938 = 0.186	0.733 × 0.610 = 0.447
2219	85	0.202 × 0.941 = 0.190	0.741 × 0.625 = 0.463

[a]From left to right the first calculated value indicates contribution of T_1-relaxation ($(1-e^{-T_R/T_1})$); the second value indicate contribution of T_2-relaxation (e^{-T_E/T_2}); the third value indicates the comprehensive contribution of both T_1- and T_2-relaxations ($(1-e^{-T_R/T_1}) \times e^{-T_E/T_2}$) to the MR signal intensities.

Accordingly, the in vitro MRI results can be understood by taking into account the different acceleration effects on T_1- and T_2-relaxations as well as the cellular release process of Gd-DOTA-CC9 in different forms. Gd-DOTA-CC9 exists in 2 distinct forms in EP-labeled hMSCs: free and clustered Gd-DOTA-CC9. It is anticipated that the free Gd-DOTA-CC9 is in favor of acceleration of T_1-relaxation of cellular water protons, and the acceleration effect on T_1-relaxation will be suppressed for the intracellular Gd-DOTA-CC9 nanoclusters. Both free and clustered Gd-DOTA-CC9 accelerate T_2-relaxation, with the latter slightly more significant.[11] The intracellular free Gd-DOTA-CC9 experienced a fast exocytosis in subsequent cell proliferation so that the T_1-relaxation rate was quickly recovered (Figure 7C), which was synchronized with the recovery of T_1-weighted signal (Figure 7A). T_2-weighted signal of hMSC EP-labeled at 2.0 and 4.0 mM exhibited further decrease after first round of cell proliferation (Figure 7B). It also reflected a decrease of contribution of T_1-relaxation rate due to exocytosis of free Gd-DOTA-CC9. The formation of Gd-DOTA-CC9 nanoclusters suppressed its acceleration effect on T_1-relaxation and induced a significant acceleration effect on T_2-relaxation. As a result, a signal reduction effect exhibited. It also significantly promoted its ICRT so that recovery of T_2-relaxation of cellular water protons was significantly slowed down (Figure 7D), which was also synchronized with the slow recovery of T_2-weighted signal intensity (Figure 7B).

Based on these findings and our previous report on EP-labeling of hMSCs with Gd-DOTA-TPP,[11] it is anticipated that EP-labeling of hMSCs with Gd-DOTA-CC9 will also render long-term tracking
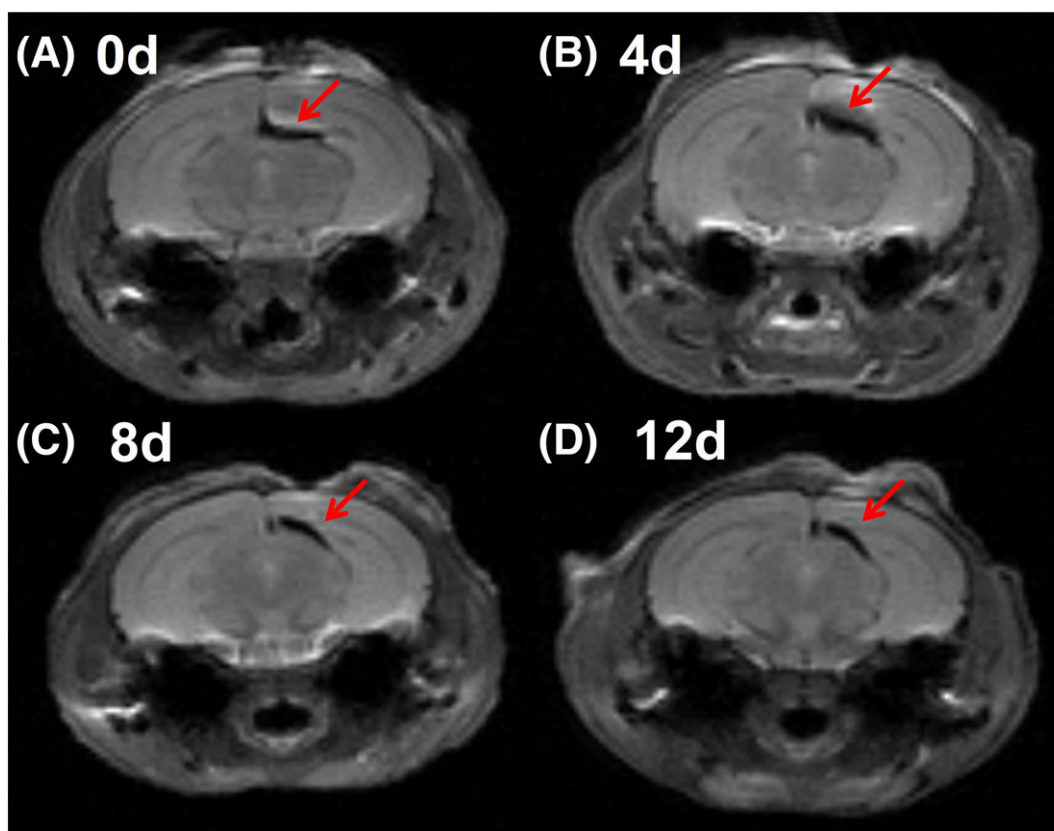
FIGURE 8 T_2-weighted magnetic resonance images of a mouse brain receiving an injection of ~4 × 10^5 human mesenchymal stem cells labeled via electroporation with Gd-DOTA-CC9 in the left ventricle as a function of 0 day (A), 4 days (B), 8 days (C), and 12 days (D) of postinjection time. An obvious dark signal existed persistently in the left ventricle (red arrows)
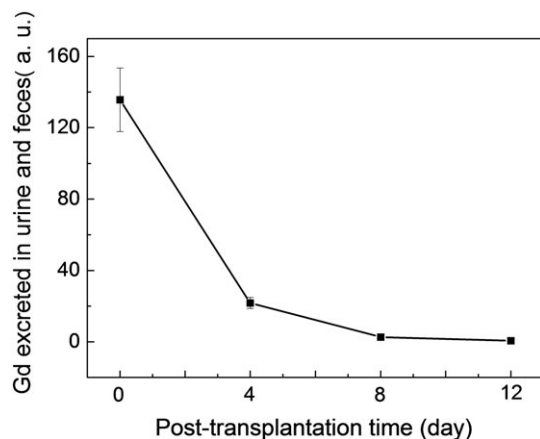
FIGURE 9 Clearance of Gd (10^{-3} mmol/kg total weight of urine and feces) from male nude mice in urine and feces as a function of different time at 0, 4, 8, and 12 days

of stem cell transplants and can provide abundant information on in vivo fates of transplanted stem cells.

3.7 | In vivo MRI of mice intracranial cell transplantation at 11.7 T

Figure 8 presents MR images of a nude mouse receiving injection of ~3.5×10^5 labeled hMSCs as a function of posttransplantation time. We note that significant dark contrast was observed at the injection site immediately after cell transplantation (Figure 8A). The contrast persisted over 12 days without obvious migration (Figure 8B-D). The in vivo results suggest that long-term tracking of stem cell transplant EP-labeled with Gd-DOTA-CC9 can be achieved with T_2-weighted MRI.

3.8 | Gadolinium concentration in organs, urine, and feces

Figure 9 presents the relative Gd concentration in mouse urine and feces as a function of posttransplantation time, which manifests the relative rate of Gd clearance. The results demonstrate a sharp decrease in Gd concentration from day 0 (immediately after cell transplantation) to day 12. The relatively higher Gd concentration in mouse feces and urine at day 0 is likely due to the fast release of free Gd-DOTA-CC9 from the labeled hMSCs. The negligible Gd concentrations at days 8 and 12 associated with the persistent dark contrast at the cell transplantation site (Figure 8C and D) imply a low clearance rate of the nanoclusters. The remaining Gd content is found to be ~164.0 ng for liver (~4.25% of total Gd introduction by cell transplantation), 28.2 ng for kidney (~0.74% of total Gd), and below the detection limit for lung.

4 | CONCLUSION

A cyclic peptide CC9 that targets MSC membrane was coupled with Gd-DOTA to yield a Gd-DOTA-CC9 complex as MRI CA. It was used to label hMSCs via EP. Electroporation-labeling of hMSCs created 2 distinct forms of Gd-DOTA-CC9 in the cytoplasm: free Gd-DOTA-

CC9 and cell-assembled nanoclusters. The former experienced fast exocytosis in subsequent cell proliferation, whereas the latter significantly promoted cell-labeling efficacy and ICRT of the agent. In vitro MRI of EP-labeled hMSCs exhibited significant signal reduction under T_2-weighted MRI, which persisted over 2 weeks. In vivo MRI demonstrated that the labeled hMSCs appeared in dark contrast after intracranial transplantation, which persisted over 12 days. The results suggest that the labeling strategy can allow long-term tracking of labeled cell transplants. Both EP-labeling and cellular uptake of Gd-DOTA-CC9 are safe in cell viability, membrane damage, ROS induction, apoptosis and necrosis, and adipogenic and osteogenic differentiation potential.

ORCID

Bo Tan http://orcid.org/0000-0003-2091-6852

REFERENCES

1. Gera A, Steinberg GK, Guzman R. In vivo neural stem cell imaging: current modalities and future directions. *Regen Med.* 2010;5(1):73-86.

2. Bulte JMW. In vivo MRI cell tracking: clinical studies. *Am J Roentgenol.* 2009;193(2):314-325.

3. Kraitchman DL, Bulte JWM. Imaging of stem cells using MRI. *Basic Res Cardiol.* 2008;103(2):105-113.

4. Bulte JWM, Zhang SC, van Gelderen P, et al. Neurotransplantation of magnetically labeled oligodendrocyte progenitors: magnetic resonance tracking of cell migration and myelination. *Proc Natl Acad Sci U S A.* 1999;96(26):15256-15261.

5. Mahmoudi M, Hosseinkhani H, Hosseinkhani M, et al. Magnetic resonance imaging tracking of stem cells in vivo using iron oxide nanoparticles as a tool for the advancement of clinical regenerative medicine. *Chem Rev.* 2011;111(2):253-280.

6. Yi PW, Chen GC, Zhang HL, et al. Magnetic resonance imaging of $Fe_3O_4@SiO_2$-labeled human mesenchymal stem cells in mice at 11.7 T. *Biomaterials.* 2013;34(12):3010-3019.

7. Terrovitis J, Stuber M, Youssef A, et al. Magnetic resonance imaging overestimates ferumoxide-labeled stem cell survival after transplantation in the heart. *Circulation.* 2008;117(12):1555-1562.

8. Agudelo CA, Tachibana Y, Hurtado AF, Ose T, Iida H, Yamaoka T. The use of magnetic resonance cell tracking to monitor endothelial progenitor cells in a rat hindlimb ischemic model. *Biomaterials.* 2012;33(8):2439-2448.

9. Tachibana Y, Enmi JI, Agudelo CA, Iida H, Yamaoka T. Long-term/bioinert labeling of rat mesenchymal stem cells with PVA-Gd conjugates and MRI monitoring of the labeled cell survival after intramuscular transplantation. *Bioconjug Chem.* 2014;25(7):1243-1251.

10. Endres PJ, MacRenaris KW, Vogt S, Meade TJ. Cell-permeable MR contrast agents with increased intracellular retention. *Bioconjug Chem.* 2008;19(10):2049-2059.

11. Zhang YH, Zhang HY, Li BB, Zhang HL, Tan B, Deng ZW. Cell-assembled (Gd-DOTA)$_i$-TPP nanoclusters as T_2 contrast agent reveal in vivo fates of stem cell transplants. *Nano Res.* 2017. in press

12. Zhang YH, Zhang HY, Ding LJ, et al. MRI reveals slow clearance of dead cell transplants in mouse forelimb muscles. *Mol Med Rep*. 2017;16(4):4068-4074.

13. Accardo A, Morisco A, Gianolio E, et al. Nanoparticles containing octreotide peptides and gadolinium complexes for MRI applications. *J Pept Sci*. 2011;17(2):154-162.

14. Morisco A, Accardo A, Gianolio E, Tesauro D, Benedetti E, Morelli G. Micelles derivatized with octreode as potential target-selective contrast agents in MRI. *J Pept Sci*. 2009;15(3):242-250.

15. De León-Rodríguez LM, Kovacs Z. The synthesis and chelation chemistry of DOTA-peptide conjugates. *Bioconjug Chem*. 2008;19(2):391-402.

16. Yoo B, Sheth VR, Pagel MD. An amine-derivatized, DOTA-loaded polymeric support for Fmoc solid phase peptide synthesis. *Tetrahedron Lett*. 2009;50(31):4459-4462.

17. Tan MQ, Lu ZR. Integrin targeted MR imaging. *Theranostics*. 2011;1:83-101.

18. Shao ZX, Zhang X, Pi YB, et al. Polycaprolactone electrospun mesh conjugated with an MSC affinity peptide for MSC homing in vivo. *Biomaterials*. 2012;33(12):3375-3387.

19. Zhao JX, Yang LP, Wang YF, Li LS, Pei XT. Development of a novel fluorogenic peptide beacon for imaging the migration of mesenchymal stem cells towards tumor in vivo. *Tissue Eng*. 2006;12:1031.

20. Cao LM, Li BB, Yi PW, et al. The interplay of T_1- and T_2-relaxiation on T_1-weighted MRI of hMSCs induced by Gd-DOTA- peptides. *Biomaterials*. 2014;35(13):4168-4174.

21. Li C, Winnard P, Bhujwalla ZM. Facile synthesis of 1-(acetic acid)-4,7,10-tris (tert-butoxycarbonylmethyl)-1,4,7,10-tetraazacyclododecane: a reactive precursor chelating agent. *Tetrahedron Lett*. 2009;50(24):2929-2931.

22. Dijkgraaf I, Kruijtzer JAW, Liu S, et al. Improved targeting of the integrin by multimerisation of RGD peptides. *Eur J Nucl Med Mol Imaging*. 2007;34(2):267-273.

23. Terreno E, Crich SG, Belfiore S, et al. Effect of the intracellular localization of a Gd-based imaging probe on the relaxation enhancement of water protons. *Magn Reson Med*. 2006;55(3):491-497.

24. McRobbie DW, Moore EA, Graves MJ, Prince MR. *MRI From Picture to Proton*. 2nd ed. New York: Cambridge University Press; 2006 Chapters 5 and 8.

SUPPORTING INFORMATION

Additional Supporting Information may be found online in the supporting information tab for this article.